Electronic Supplementary Material (ESI) for New Journal of Chemistry.

ELECTRONIC SUPPLEMENTARY INFORMATION

Upconverting Er^{3+}, Yb^{3+} activated β-$NaYF_4$ thin films: a solution route using a novel sodium β-diketonate polyether adduct

Maria R. Catalano,[a] Anna L. Pellegrino,[a] Patrizia Rossi,[b] Paola Paoli,[b] Paolo Cortelletti,[c] Marco Pedroni,[c] Adolfo Speghini,[c,*] and Graziella Malandrino[a,*]

a) Dipartimento di Scienze Chimiche, University of Catania and INSTM UdR Catania, V.le A. Doria 6, 95125 Catania, Italy
b) Dipartimento di Ingegneria Industriale, Università di Firenze, Via Santa Marta 3, 50139 Firenze, Italy
c) Dipartimento di Biotecnologie, Università di Verona and INSTM UdR Verona, Strada le Grazie 15, 37134 Verona, Italy

Precursor synthesis and characterization. The Na(hfa)•tetraglyme adducts has been prepared by the reaction of NaOH (0.45 gr; 1.12×10^{-2} mol) suspended in dichloromethane (30 ml) with tetraglyme (1.57 g, 7.07×10^{-3} mol) and H-hfa (1.470 g, 7.07×10^{-3} mol). The mixture was refluxed, under stirring, for 1 h. The solution was collected by filtration under vacuum and the excess of NaOH was filtered off. White crystals were obtained upon evaporation of the solvent, were washed two times in pentane and recovered by filtration. The reaction yield was 87 %. The melting point of the crude product was 65-67 °C/760 Torr.

The FT-IR transmittance spectrum of the Na(hfa)•tetraglyme was recorded using a FT-IR-430 JASCO spectrometer as nujol mull of the sample placed between NaCl plates. The spectrum (Figure S1) shows the peaks at 1674 cm^{-1} and at 1560 associated with C=O stretching and C=C stretching respectively, due to the β-diketonate ligand. The broad band observed in the 1000-1300 cm^{-1} range may be associated with absorptions of the polyether C-O bending and/or stretching overlapped with the C-F stretching. In addition, bands at 1015, 861 and 837 cm^{-1} can be associated with glyme modes. The C-H glyme stretching modes, lying in the 2800-3000 cm^{-1} range, overlap with nujol features. In fact, the nujol shows peaks at 2923 cm^{-1}, at 1461 cm^{-1} and at 1377 cm^{-1}. The absence of any bands around 3500 cm^{-1} range confirms the absence of coordinated water molecules, indicating that the Lewis base glyme saturates the metal center.

^{1}H NMR and ^{13}C-NMR spectra were recorded on a Varian Inova 500 spectrometer. The ^{1}H -NMR and ^{13}C-NMR characterizations (Figure S2a) confirm the formation of the desired complex; in fact the ^{1}H NMR spectrum of the Na(hfa)•tetraglyme adduct shows two singlet at δ=5.08 and 3.4 ppm due to the one proton of the hfa ligand and to the six equivalent proton of the two methyl groups of the tetraglyme ligand, respectively. In addition to the singlet, the multiplet at δ=3.5-3.7 represent resonances of methylenic protons of the tetraglyme. The single peak at 7.2 ppm is due to the chloroform.

The ^{13}C NMR spectrum (Figure S2b) shows resonances at δ= 86 ppm, 118 ppm e 176 ppm associated, respectively, with a singlet for the *C*H groups, a quartet for the *C*F_3 groups and a quartet for the *C*O groups of the coordinated hfa ligands consist. The quartets are due to first order (CF_3; ^{1}J = 284 Hz) and second order (CO; ^{2}J = 33 Hz) coupling with the CF_3 fluorine atoms. Coordinated tetraglyme give signals at δ= 59, due to methylic carbons (s, O*C*H_3,), in the range of δ=69 - 71 there are the signal due to eight methylenic carbons.

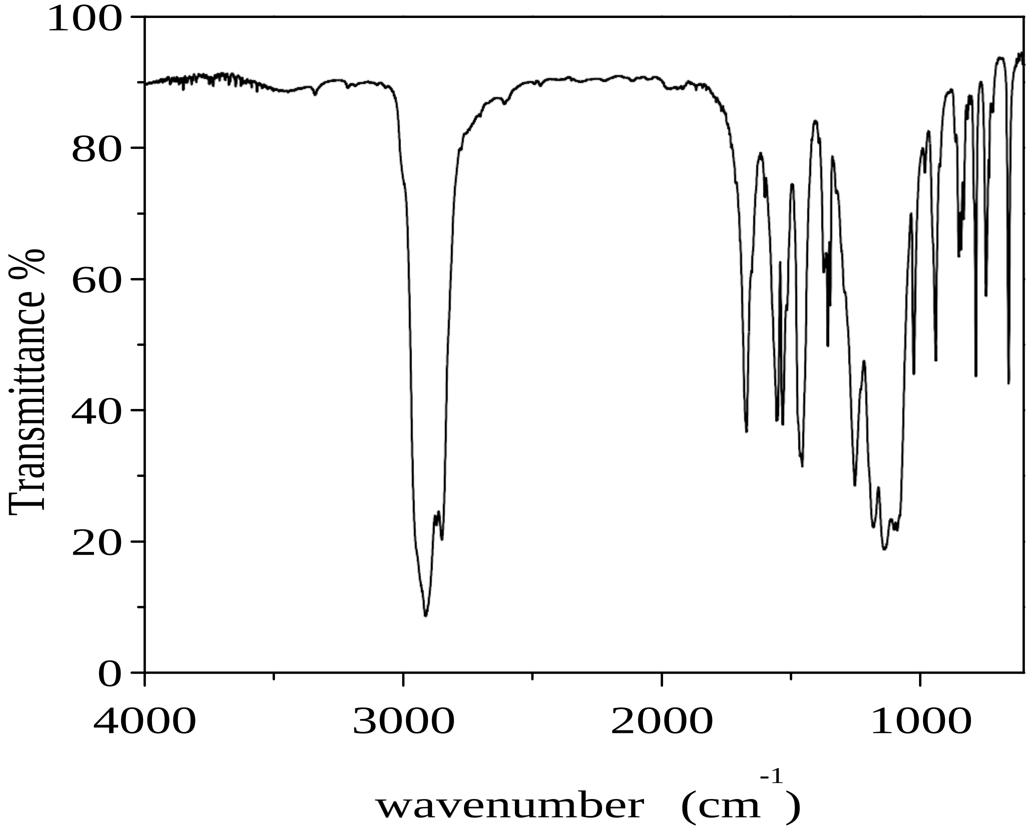

Figure S1. FTIR transmittance spectrum of the Na(hfa) •tetraglyme adduct.

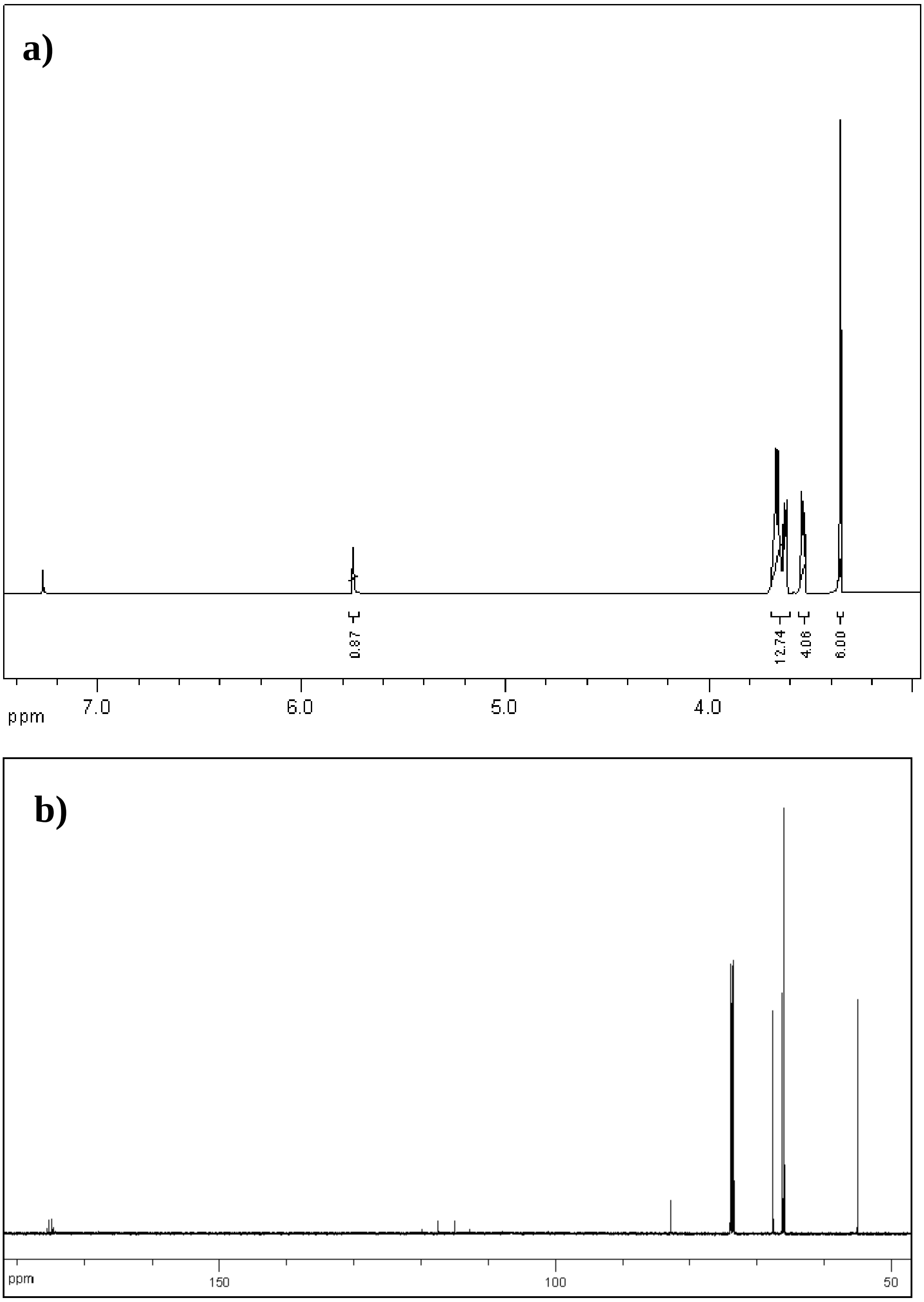

Figure S2. ^{1}H-NMR (a) and ^{13}C-NMR (b) spectra of the Na(hfa) •tetraglyme adduct

Thermogravimetric analyses were performed using a Mettler Toledo TGA/SDTA 851^{e} on samples which weight was between 5 and 13 mg (TGA). Thermal measurements were made under prepurified nitrogen flow fed into the working chamber at 30 sccm, with a 5°C/min heating rate. The atmospheric pressure thermal gravimetric analysis (Figure S3a) reveals that the weight loss takes place in a single step, in the 130-250°C. The differential scanning calorimetric data (Figure S3b) show endothermic peaks at 43°C, most probably associated with a solid-solid phase change, and at 67°C due to the melting of the adduct, while the peak at a higher temperature is likely due to exothermic processes associated with the ligand loss.

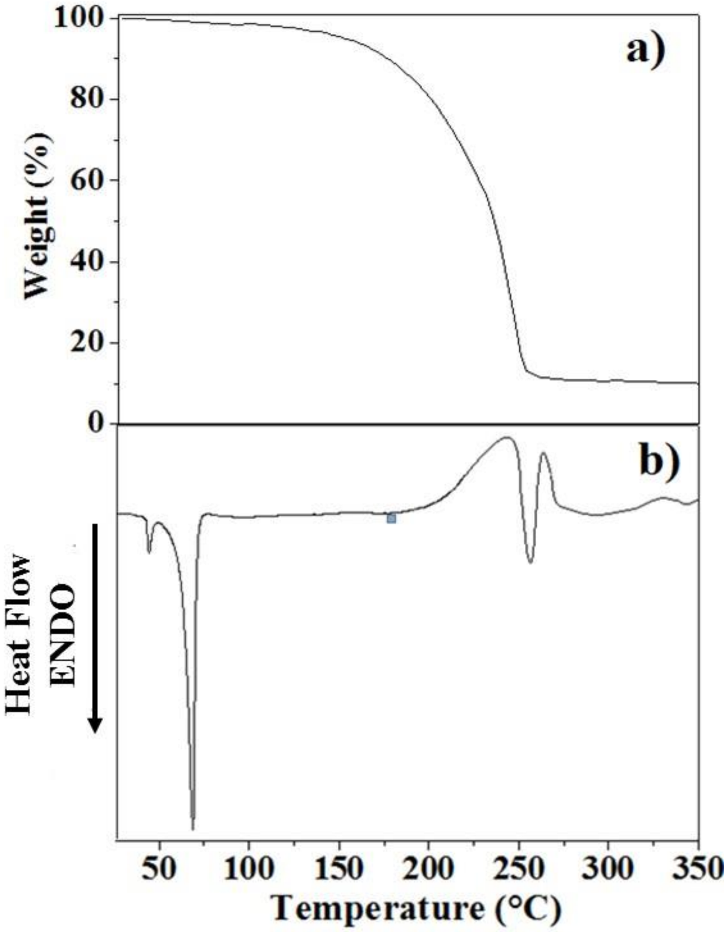

Figure S3. TGA (a) and DSC (b) of the Na(hfa)•tetraglyme adduct.

Single crystal structure. Na(hfa)•tetraglyme was investigated, at the solid state, by means of single crystal X-ray diffraction (SCXRD). SCXRD measurements were carried out with an Oxford Diffraction Excalibur diffractometer using the Cu-K_α radiation (λ = 1.54184 Å). Data collection was performed with the program CrysAlis CCD.[1] Data reduction was carried out with the program CrysAlis RED.[1] Finally, absorption corrections was performed with the program ABSPACK in CrysAlis RED.

The structure was solved by using the SIR-97 package[2] and subsequently refined on the F^2 values by the full-matrix least-squares program SHELXL-97.[3]

Geometrical calculations were performed by PARST97,[4] and molecular plots were produced by the programs ORTEP-3[5] and Discovery Studio Visualizer (v4.5).[6]

In Table S1 crystal data and refinement parameters of the investigated structure are reported.

In Na(hfa)•tetraglyme, the tetraglyme molecule is disordered. Such disorder was modelled by introducing double positions (“a” and “b” in the following), with an occupancy factor of 0.74/0.26, respectively. The non-hydrogen atoms of such molecule were isotropically refined. The hydrogen atoms of the tetraglyme molecule, as well as that of the hfa anion, were set in calculated positions and refined in agreement with the carbon atoms to which they are bonded. In addition, the two CF_3 groups of the hfa anion are in disordered positions that were modelled introducing three positions for the fluorine atoms (occupancy factors 0.39, 036 and 0.25), such atoms were then isotropically refined.

Table S1: Crystallographic data and refinement parameters for Na(hfa)•tetraglyme.

	Na(hfa)•tetraglyme
Empirical formula	$C_{15}H_{23}F_6NaO_7$
Formula weight	452.32
Temperature (K)	150
Wavelength (Å)	1.54184
Crystal system, space group	Triclinic, P-1
Unit cell dimensions (Å, °)	a = 8.8042(5), α = 106.022(5) b = 9.8572(6), β = 103.017(5) c = 13.1313(8), γ = 102.921(5)
Volume ($Å^3$)	1016.3(1)
Z, Dc (mg/cm^3)	2, 1.478
μ(mm-1)	1.500
F(000)	468
Crystal size (mm)	0.23 x 0.28 x 0.32
θ range (°)	4.902 – 70.618
Reflections collected / unique	10514 / 3710
Data / parameters	3710 / 419
Goodness-of-fit on F^2	1.029
Final R indices [I>2σ(I)]	0.0379 / 0.0927
R indices (all data)	0.0558 / 0.1041

Table S2. Selected bond lengths distances (Å) and angles (°) in Na(hfa)•tetraglyme

	Distances (Å)
Na(1)-O(1)	2.354(1)
Na(1)-O(2)	2.341(1)
Na(1)-O(3)[1]	2.833(4) / 2.65(2)
Na(1)-O(4)	2.503(2) / 2.448(9)
Na(1)-O(5)	2.599(4) / 2.90(1)
Na(1)-O(6)	2.566(8) / 2.37(3)
Na(1)-O(7)	2.476(9) / 2.41(3)
	Angles (°)
O(1)-Na(1)-O(2)	76.66(5)
O(1)-Na(1)-O(3)	76.60(8) / 77.3(3)
O(1)-Na(1)-O(4)	90.82(7) / 86.8(2)
O(1)-Na(1)-O(5)	145.9(1) / 149.4(3)
O(1)-Na(1)-O(6)	138.7(2) / 141.8(9)
O(1)-Na(1)-O(7)	87.9(2) / 91.2(8)
O(2)-Na(1)-O(3)	146.62(8)/ 139.6(3)
O(2)-Na(1)-O(4)	98.26(8) / 80.6(2)
O(2)-Na(1)-O(5)	83.87(8) / 90.3(3)
O(2)-Na(1)-O(6)	84.1(3) / 86(1)
O(2)-Na(1)-O(7)	110.6(2) / 116.5(6)
O(3)-Na(1)-O(4)	62.59(8) / 67.6(3)
O(3)-Na(1)-O(5)	108.3(1) / 96.8(4)
O(3)-Na(1)-O(6)	129.3(3) / 132(1)
O(3)-Na(1)-O(7)	87.9(2) / 94.3(7)
O(4)-Na(1)-O(5)	64.4(1) / 63.6(4)
O(4)-Na(1)-O(6)	128.3(2) / 124(1)
O(4)-Na(1)-O(7)	149.9(2) / 161.9(7)
O(5)-Na(1)-O(6)	64.5(3) / 62(1)
O(5)-Na(1)-O(7)	125.4(2) / 119.4(8)
O(6)-Na(1)-O(7)	65.2(3) / 67(1)

[1] = due to the disorder affecting the tetraglyme molecule for each Na(1)-$O_{tetraglyme}$ distance and angle two value are reported for the "a" and "b" models, respectively.

Table S3. Dihedral angles in the tetraglyme molecules in Na(hfa)•tetraglyme

	a[1]	b
C(6)-O(3)-C(7)-C(8)	-170.6(4)	-174(2)
O(3)-C(7)-C(8)-O(4)	-68.1(5)	-80(1)
C(7)-C(8)-O(4)-C(9)	173.6(4)	-177(1)
C(8)-O(4)-C(9)-C(10)	-167.5(3)	-73(2)
O(4)-C(9)-C(10)-O(5)	59.7(4)	-51(2)
C(9)-C(10)-O(5)-C(11)	179.5(5)	-86(2)
C(10)-O(5)-C(11)-C(12)	176.5(6)	-179(2)
O(5)-C(11)-C(12)-O(6)	-64(1)	-63(4)
C(11)-C(12)-O(6)-C(13)	167.1(9)	166(4)
C(12)-O(6)-C(13)-C(14)	175.1(9)	169(4)
O(6)-C(13)-C(14)-O(7)	55(1)	50(5)
C(13)-C(14)-O(7)-C(15)	170.8(8)	-175(3)

[1] = due to the disorder affecting the tetraglyme molecule for each dihedral angle two values are reported for the “a” and “b” models, respectively.

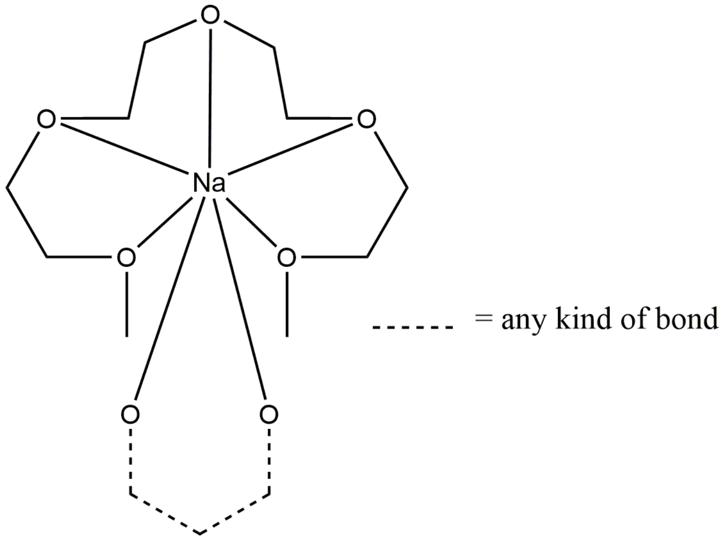

Scheme S1. Fragment searched in the CSD

Film synthesis and characterization. Films were synthesized using a sol-gel route with the following molar ratio 0.8 Y(hfa)$_3$•diglyme : 0.2 Yb(hfa)$_3$•diglyme : 0.04 Er(hfa)$_3$•diglyme : 1 Na(hfa)•tetraglyme : 43.5 C_2H_5OH : 1.5 H_2O : 0.4 CF_3COOH.

The solution was left aging at 60 °C for 20 h and successively applied through spin-coating in four subsequent steps on Si (001) or quartz substrates. For each step 0.2 ml of the gel were spinned at 3000 RPM and for 60 s. After each step, the sample was heated at 400°C in air for 10 min. This procedure of spinning and heating was repeated four times. Finally, the film was annealed at 400 °C in air for 1 h. The spin coating was carried out using a SPIN-150, SPS EUROPE apparatus.

Samples were characterized by X-ray diffraction (XRD) in the Bragg–Brentano configuration using a θ-θ Bruker–AXS D5005 diffractometer equipped with a Göebel mirror to parallel the Cu K_α radiation (0.15418 nm) operating at 40 kV and 30 mA.

In figure S4, the pattern of the films is reported with the relative theoretical peak positions for the β-hexagonal $NaYF_4$ phase (red lines), α-cubic $NaYF_4$ phase (blue lines), and NaF (green lines).

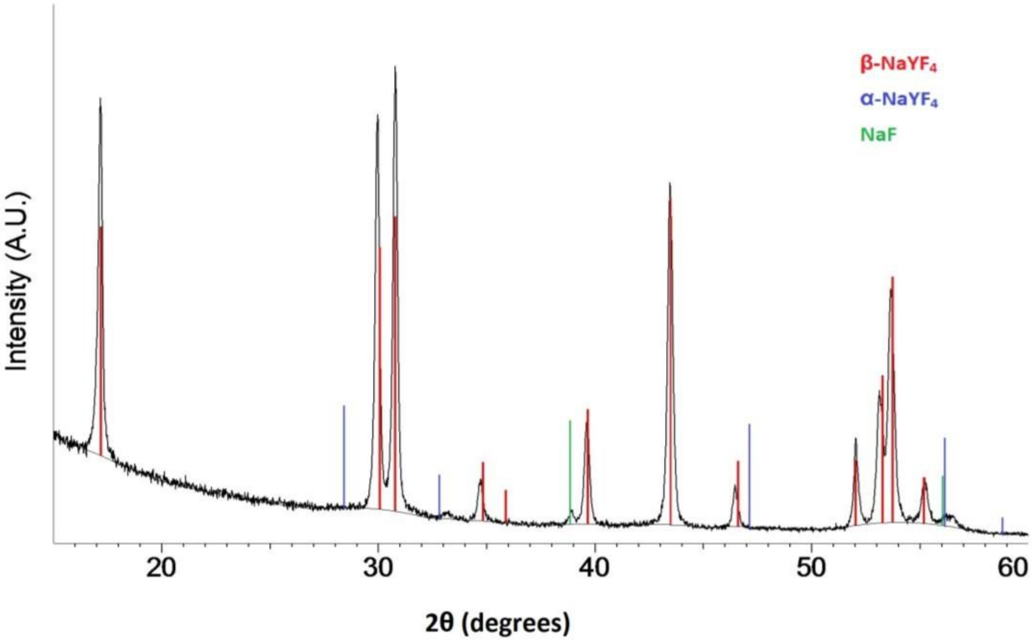

Fig. S4. XRD pattern of the $NaYF_4$ film doped Yb^{3+}/Er^{3+}.

Film morphology was observed by field-emission scanning electron microscopy (FE-SEM) using a ZEISS SUPRA VP 55 microscope. A low magnification image is reported in Fig. S5.

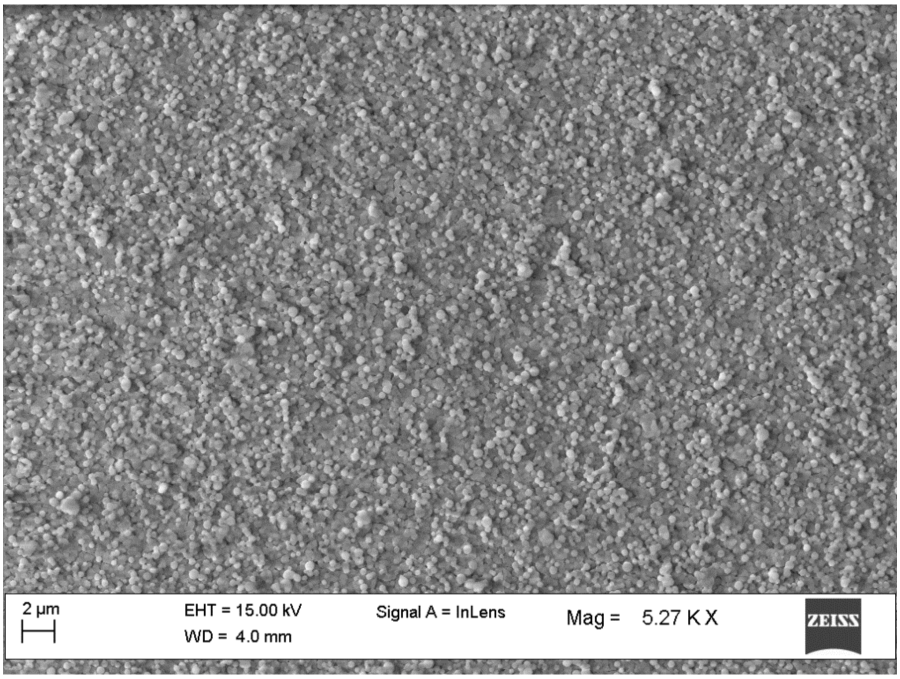

Fig. S5. Low Magnification FE-SEM image of the NaYF4 film doped Yb3+/Er3+

The energy dispersive X-Ray spectrum (Fig. S5) shows the typical peaks of the Na,Y, and Yb elements. The Na K_α peak is observed at 1.06 keV, the Y L_α and L_β peaks are observed in the range 1.8-2.2 keV; the peak at 1.6 KeV is due to Yb L_α, while the peaks in the 7.5 -8.5 range are due to the M_α and M_β Yb lines.
In addition, the windowless EDX detector allowed to detect the F K_α peak at 0.670 keV. The small peak at 0.520 keV is associated with the O K_α peak, due to the SiO_2 present on the Si surface.

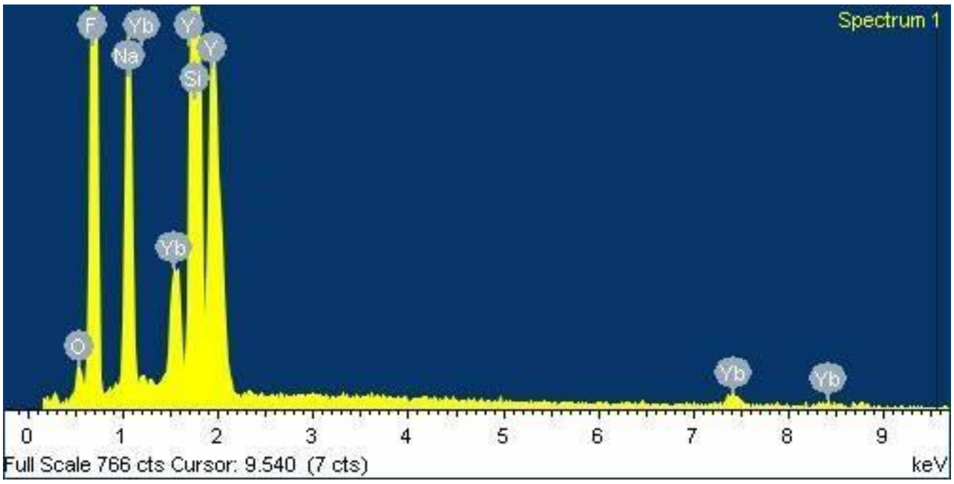

Fig. S6. EDX analysis of the $NaYF_4$ film doped Yb^{3+}/Er^{3+}.

Spectroscopic measurements. Room temperature upconversion emission spectrum and time resolved upconversion emission curves of the sample were obtained using a 980 nm diode laser system (diode laser: CNI Optoelectronics Tech; pulse generator: Arduino Uno microcontroller) as the excitation source, in continuous wave and pulsed mode. The emission signal was analysed by a half-meter monochromator (HR460, Jobin Yvon) equipped with a 1200 lines/mm grating and detected with a CCD detector (Spectrum One, Jobin Yvon). The spectral resolution of the emission spectra is 0.2 nm. The emission decay curves were recorded upon pulsed diode laser excitation (@10 Hz) and detected with a GaAs photomultiplier (Hamamatsu) and a 500 MHz digital oscilloscope (WaveRunner, LeCroy).

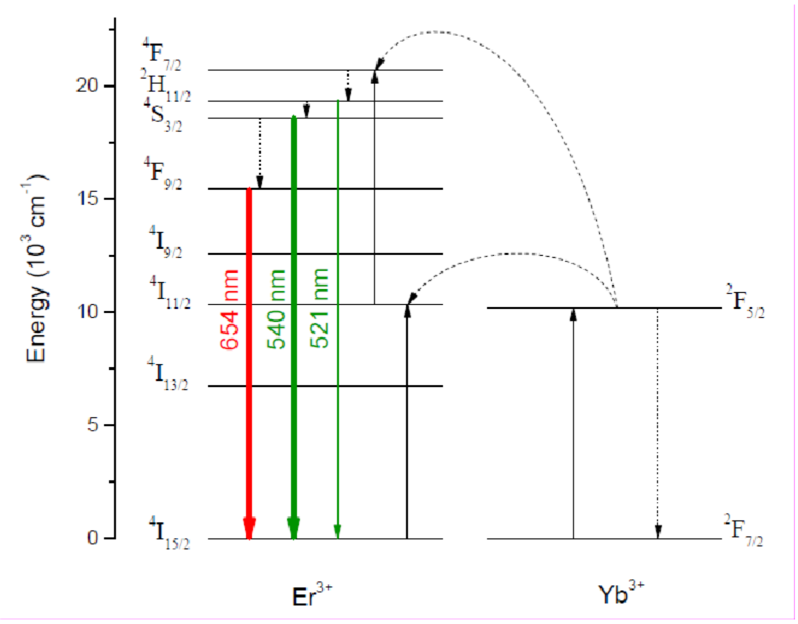

Fig. S7. Energy level diagrams for Er^{3+} and Yb^{3+} ions and Energy Transfer Upconversion (ETU) mechanism upon 980 nm laser excitation. For this mechanism, Yb^{3+} ions are excited by 980 photons, and then energy transfer from Yb^{3+} ions to Er^{3+} take place. Due to the high percentage of the Yb^{3+} ions (20 mol%) with respect to the total metal content, the main mechanism for the upconversion process is most probably Energy Transfer Upconversion (ETU).[7]

---

[1] CrysAlisPro, Agilent Technologies (2011).

[2] A. Altomare, G. L. Cascarano, C. Giacovazzo, A. Guagliardi, A. G. Moliterni, M. C. Burla, G. Polidori, M. Camalli, R. Spagna, *J. Appl. Cryst.*, **1999**, *32*, 115.

[3] Sheldrick, G. M. *SHELX 97*, University of Göttingen, Germany, **1997**.

[4] M. Nardelli, *J. Appl. Cryst*, **1995**, *28*, 659.

[5] L. J. Farrugia, *J. Appl. Cryst*, **1997**, *30*, 565.

[6] Dassault Systèmes BIOVIA, Discovery Studio Visualizer, Release 4.5, San Diego: Dassault Systèmes, 2015.

[7] A. Bednarkiewicz, D. Wawrzynczyk, A. Gagor, L. Kepinski, M. Kurnatowska, L. Krajczyk, M. Nyk, M. Samoc, W. Strek, Nanotechnology 23 (2012) p.145705.